Process Safety and Environmental Protection 192 (2024) 1330–1343

Contents lists available at ScienceDirect

Process Safety and Environmental Protection

journal homepage: www.journals.elsevier.com/process-safety-and-environmental-protection

Exploring experimental tests concerning liquid hydrogen releases

Federica Tamburini [a,b,*], Martin Kluge [c], Abdel Karim Habib [c], Federico Ustolin [b], Valerio Cozzani [a], Nicola Paltrinieri [b]

[a] LISES – Department of Civil, Chemical, Environmental, and Materials Engineering, Alma Mater Studiorum – University of Bologna, via Terracini 28, Bologna 40131, Italy
[b] Department of Mechanical and Industrial Engineering, Norwegian University of Science and Technology NTNU, Trondheim 7491, Norway
[c] Bundesanstalt für Materialforschung und –prüfung, Unter den Eichen 87, Berlin 12205, Germany

ARTICLE INFO

Keywords:
Liquid Hydrogen
Experimental test
Rapid phase transition
Ignition
Safety

ABSTRACT

In recent years, the adoption of liquid hydrogen (LH_2) has increased significantly in industrial and transport applications, driven by its low carbon footprint, thereby aiding the fight against global warming. Additionally, its high volumetric energy density, compared to gaseous or compressed hydrogen, enhances hydrogen storage capabilities. However, safety remains a major concern due to its physical-chemical properties and inherent hazardous characteristics, especially in the event of spillage scenarios. Therefore, to better understand the consequences of LH_2 releases onto or into water, large-scale experimental tests were conducted by Bundesanstalt für Materialforschung und -prüfung (BAM) within the Safe Hydrogen Fuel Handling and Use for Efficient Implementation (SH_2IFT) project at the Test Site Technical Safety of BAM, comprising 75 single spill events at varied release rates and orientations. While the rapid phase transition (RPT) phenomenon was not observed, self-ignition of the hydrogen-air cloud occurred, accompanied by blast wave overpressure and heat radiation, without a discernible ignition source. These findings emphasize the need for further investigation into LH_2 safety. Leveraging experimental data for real-world applications provides insights into safe LH_2 infrastructure implementation, laying foundational knowledge for addressing safety challenges and advancing LH_2 technology.

1. Introduction

Lately, international concern around global warming issue is growing fast (IEA, 2023; Tamburini et al., 2024d; Wang et al., 2023). Authorities and organizations are implementing strategic tasks towards climate change effects mitigation in different economic areas (Fawzy et al., 2020), including generation of electricity and heat as well as end uses in buildings, transportation, and manufacturing and construction (Abbass et al., 2022; Nukusheva et al., 2021). Among the various energy solutions, hydrogen (H_2) is believed to be a valid alternative to pursue ambitious decarbonization policies aimed at reducing greenhouse gas emissions and establishing a zero-carbon society (Hassan et al., 2024; Olabi et al., 2023; Reigstad et al., 2022; Tamburini et al., 2023a). It offers a versatile, low-carbon energy carrier that can be produced from renewable sources and efficiently converted, stored, and utilized, thus unfolding a broad spectrum of possibilities for future applications (Aziz, 2021; Pleshivtseva et al., 2023). This capability complements other decarbonization technologies like Carbon Capture and Storage (CCS) (Tamburini et al., 2024b), significantly reducing emissions across industries, aiding in the transition to a sustainable energy future (IPCC, 2005; Tamburini et al., 2024a).

In the field of long-distance transport and storage, liquid hydrogen (LH_2) holds particular significance due to its high energy density and relatively low weight (Aziz, 2021; Zhang et al., 2023). This makes it a viable option for applications such as fueling long-haul vehicles, powering maritime vessels, and facilitating energy export across regions (Mangold et al., 2022; Ustolin et al., 2022). The ability to liquefy hydrogen enables efficient storage and transport, overcoming some of the limitations associated with gaseous or compressed hydrogen (e.g., large transfer volumes), thus unlocking opportunities for widespread adoption in various sectors (Ahluwalia et al., 2023; Hansen, 2020). As efforts intensify to decarbonize transportation and industrial processes on a global scale, the role of LH_2 as an adaptable, clean energy carrier becomes crucial (Berstad et al., 2022; Tamburini et al., 2023b).

* Corresponding author at: LISES – Department of Civil, Chemical, Environmental, and Materials Engineering, Alma Mater Studiorum – University of Bologna, via Terracini 28, Bologna 40131, Italy.
E-mail address: federica.tamburini9@unibo.it (F. Tamburini).

https://doi.org/10.1016/j.psep.2024.11.014
Received 15 June 2024; Received in revised form 19 October 2024; Accepted 4 November 2024
Available online 5 November 2024

Fig. 1. Experimental test set-up at the Test Site Technical Safety of BAM to investigate LH_2 releases above and underwater. From left to right, the water basin equipped with the release mechanism and instrumentation, a cabin adapted for logging equipment, and the LH_2 delivery truck.

Thereby, it is fundamental to address the array of safety concerns attendant upon its adoption, particularly related to its intrinsic hazardous characteristics (Abohamzeh et al., 2021; Tamburini et al., 2024c). LH_2 presents a volatile nature, characterized by a low ignition energy (0.02 mJ), a wide flammability range (in air) (4 ÷ 77 vol%), a wide detonation range (18 ÷ 59 vol%), and a high susceptibility to material embrittlement upon contact (Habib et al., 2022; Li et al., 2022; Shu et al., 2022; Ustolin et al., 2020b). In case of spillage scenarios, the rapid evaporation of liquid hydrogen creates the formation of highly combustible vapor clouds, escalating the risk of explosions (Pasman and Rogers, 2012; Rong et al., 2023). Moreover, in case of releases above water, the phenomenon of rapid phase transition (RPT) might contribute with additional scenarios to the complexity of LH_2 spill events (Odsæter et al., 2021). As there is historical evidence of liquified natural gas (LNG) RPTs, the probability of LH_2 RPTs is deemed possible as well, given their similar cryogenic peculiarities (Ødegård et al., 2022). RPT consequences involve strong physical explosions arising from the rapid vaporization that follows the encounter between liquids with broadly divergent temperatures and boiling points (e.g., LH_2 at −253 °C (or LNG at −163 °C) and water at ambient conditions) (Aursand and Hammer, 2018; Salzano et al., 2020). Furthermore, based on when and where the RPT occurs during a leakage event, early or delayed RPT may occur (Ustolin et al., 2020a). Early RPT is defined as any RPT occurring after a few seconds near the point of impact while delayed RPT consists of any RPT occurring somewhere in the spreading pool also after tens of seconds (Ødegård et al., 2022).

Experimental research into RPT of LH_2 following spill events onto or into water is limited. (Atkinson, 2020) investigated the consequences of spraying water onto a pool of LH_2 while (Verfondern and Dienhart, 2007) analysed the effects of spreading LH_2 above water. None of these experiments identified RPTs during their tests. A potential explanation behind the unprobeable LH_2 RPTs relies on the low Leidenfrost temperature of LH_2 that prevents the collapse of a vapour film separating LH_2 and water (Odsæter et al., 2021; Ustolin et al., 2020a). Additionally, (Odsæter et al., 2021), through simulations, suggested that delayed LH_2 RPTs are very unlikely, and that early RPT is less likely to occur for LH_2 than for LNG. However, the small number of experiments did not allow to confirm this theory with certainty. In 2020, a series of experiments were performed by BAM under the Safe Hydrogen Fuel Handling and Use for Efficient Implementation (SH_2IFT) project on the Test Site Technical Safety of BAM, with the aim of investigating whether early RPTs are possible when releasing a LH_2 jet onto water or underwater (Ødegård et al., 2022).

In the present paper, the results of this experimental campaign, in terms of pressure, temperature, H_2 concentration, and heat radiation, were collected, examined, and discussed. Both the outcomes associated with single LH_2 releases and those derived from aggregating different trials based on specific variables were reported and analysed. Given that these large-scale experiments were designed to simulate realistic conditions during LH_2 filling operations, the illustrated datasets aim to enhance competency within the safety of hydrogen technology, particularly in the context of maritime transportation, where the handling and utilization of large volumes of LH_2 are critical.

The following part of the paper is structured as follows. In Section 2, the experimental tests configuration is presented in terms of test field description, set-up of the instrumentation, and test campaign. Furthermore, the tools adopted for data analysis are introduced. Then, Section 3 illustrates and discusses the results of the experimental trials focusing on both single and aggregated test outputs. Finally, some conclusive remarks are outlined in Section 4.

2. Experimental section

2.1. Experimental test field

The experimental studies on the releases of LH_2 onto or underwater were carried out by Bundesanstalt für Materialforschung und –prüfung (BAM) at the Test Site Technical Safety in Horstwalde, Germany. LH_2, stored up to 10 bar, was delivered from a 40 m^3 tanker truck, totalling 2.5 t of LH_2, using a 46 m-long flexible transfer line with a 20 mm outlet nozzle. The transfer line consisted of a double-walled, vacuum-insulated hose and vacuum-insulated valves, suitable for cryogenic applications (Ødegård et al., 2022).

LH_2 was delivered to a fresh water tarpaulin-lined basin with a

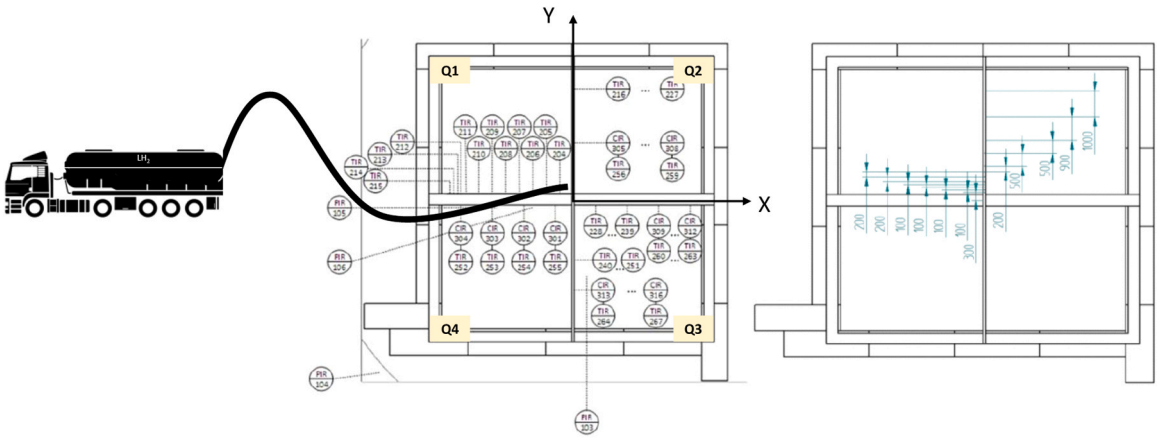

Fig. 2. Set-up of the sensors deployed around the basin (TIR = Thermocouple, CIR = Gas sensor, PIR = Blast sensor), with associated distances (quotes in mm).

capacity of 150 m^3 (10 m x 10 m x 1.5 m) to simulate real-world conditions as accurately as possible. This volume of water allows for the replication of open water conditions, facilitating efficient heat transfer to prevent excessive cooling during the short-term (up to two minutes) release experiments (Ødegård et al., 2022).

The release of LH_2 was facilitated by a manually operated valve at the trailer, providing control over the release rate. The outlet nozzle could be adjusted to various orientations relative to the water surface and could also be submerged, allowing for a wide range of experimental tests. Additionally, an emergency release point was integrated into the release system. Helium was used to purge the infrastructure before the start of each release event and grounding operations were performed to avoid any potential ignition sources resulting from electrostatic discharges.

The entire experimental set-up is illustrated in Fig. 1.

2.2. Test instrumentation set-up

A variety of sensors were deployed around the basin (Ødegård et al., 2022; Tamburini et al., 2023c) to obtain specific measurements during the experimental tests. Specifically, 64 K-type thermocouples (TIRs) were positioned alternately 10 cm above and 10 cm beneath the water surface to measure air and water temperature. In addition, a thermocouple was placed directly at the nozzle. Four pressure sensors (PIRs) were strategically located to measure blast overpressures, both underwater (PIR 105, 3 m away from the release point; PIR 106, 2 m away from the release point) and above the water surface (PIR 103, 3 m away from the release point; PIR 104, 10 m away from the release point). Furthermore, H_2 concentration probes (CIRs) at 17 different locations were utilized. These sensors can detect hydrogen concentrations in air within the range of 0–100 vol% (NEOHYSENS NEO974A) and with a response time of approximately 1 s. Finally, three bolometers (Medtherm 64-XX-14) located at distances of 70 m, 90 m, and 110 m from the point of the release were used for heat radiation measurements.

In Fig. 2, the arrangement of thermocouples (TIRs), concentration probes (CIRs), and blast sensors (PIRs) around the four quadrants (i.e., Q1, Q2, Q3, and Q4) of the basin is depicted.

For clarity purposes, Table 1 provides the exact coordinates of thermocouples, concentration sensors, pressure sensors, and bolometers around the basin, assuming as centre of the coordinates the LH_2 release point (see Fig. 2). Sensor positioning in relation to the water surface is indicated with two signs: (+) to indicate that the sensor is located 10 cm above the water surface and (-) to indicate that the sensor is located 10 cm below the water surface.

Additional useful measurements were performed: a weighing system composed of four 10-t load cells (MTS VC 3500 - accuracy +/- 1.5 kg) was placed under the tanker truck to determine the mass released during each trial, and two ultra-sonic anemometers (USA, Typ Metek USA-1 Scientific) were mounted at two opposite corners (in Q2 and Q4) of the basin to record wind speed and direction data. Finally, the set-up was equipped with eight standard cameras (Typ GoPro Gen. 3 – 8), a high-speed camera, an infrared camera (FLIR E95), and an unmanned aerial vehicle (UAV) equipped with regular (DJI M300 RTK) and infrared (DJI Zenmuse H20T) camera systems for video recording.

2.3. Experimental campaign

The test schedule involved 75 LH_2 releases, all performed and successfully documented, for a total of 24 trials, each consisting of multiple releases (Habib et al., 2022). Thanks to the characteristics of the outlet nozzle, three distinct release locations and orientations were investigated: 50 cm above the water surface oriented vertically downward (AV), 30 cm under the water surface oriented vertically downward (UV), and 30 cm under the water surface oriented horizontally parallel to the water (UH) (Habib et al., 2022).

A summary of the trials is reported in Table 2, including the number of overall and reliable releases, the type of release in terms of orientation and location (i.e., AV, UV, or UH), and the range of mass outflow rate. Due to the accuracy of the weighing system, only releases with a duration of more than 10 s and a mass of more than 5 kg can be considered reliable regarding the mass flow. It is worth noting that Trial 018 is omitted from the list as it was not recorded due to a malfunction of the logging system and is therefore considered “failed”. Trial 019 represents the re-simulation of the failed Trial 018.

2.4. Data analysis

The Savitzky-Golay filter was implemented to advance signal processing in the domain of thermocouples, blast probes, gas concentration sensors, and bolometers measurements (Menon and Seelamantula, 2014). This curve-fitting technique represents a crucial method for noise reduction and signal enhancement, employing local polynomial regression within sliding windows to effectively smooth noisy data while preserving essential signal characteristics. Mathematically, the Savitzky-Golay filter minimizes the least squares error between the data and a polynomial fit within each window, thereby mitigating the effects of noise and artifacts inherent in measurements obtained from sensors operating in harsh environments (John et al., 2021). This approach was selected given its suitability in scenarios where accurate detection of subtle changes in temperature, pressure, concentration, or heat radiation is essential, such as in ignition studies, industrial process monitoring, and environmental sensing applications (Isnanto, 2011).

In the present paper, the MATLAB function “*sgolay*” associated with the Savitzky-Golay filter was adopted (The MathWorks Inc, 2024). By

Table 1
Coordinates of all the sensors located around the basin ((+), sensor located 10 cm above the water surface; (-), sensor located 10 cm below the water surface).

Sensor	X [m]	Y [m]	Location with respect to the water surface
Thermocouple/Concentration sensor			
TIR 204	−0.30	0	(+)
TIR 205	−0.40	0	(-)
TIR 206	−0.50	0	(+)
TIR 207	−0.60	0	(-)
TIR 208	−0.70	0	(+)
TIR 209	−0.90	0	(-)
TIR 210	−1.10	0	(+)
TIR 211	−1.60	0	(-)
TIR 212	−2.10	0	(+)
TIR 213	−3.00	0	(-)
TIR 214	−4.00	0	(+)
TIR 215	−5.00	0	(-)
TIR 216	0	5.00	(+)
TIR 217	0	4.00	(-)
TIR 218	0	3.00	(+)
TIR 219	0	2.10	(-)
TIR 220	0	1.60	(+)
TIR 221	0	1.10	(-)
TIR 222	0	0.90	(+)
TIR 223	0	0.70	(-)
TIR 224	0	0.60	(+)
TIR 225	0	0.50	(-)
TIR 226	0	0.40	(+)
TIR 227	0	0.30	(-)
TIR 228	0.30	0	(+)
TIR 229	0.40	0	(-)
TIR 230	0.50	0	(+)
TIR 231	0.60	0	(-)
TIR 232	0.70	0	(+)
TIR 233	0.90	0	(-)
TIR 234	1.10	0	(+)
TIR 235	1.60	0	(-)
TIR 236	2.10	0	(+)
TIR 237	3.00	0	(-)
TIR 238	4.00	0	(+)
TIR 239	5.00	0	(-)
TIR 240	0	−0.30	(+)
TIR 241	0	−0.40	(-)
TIR 242	0	−0.50	(+)
TIR 243	0	−0.60	(-)
TIR 244	0	−0.70	(+)
TIR 245	0	−0.90	(-)
TIR 246	0	−1.10	(+)
TIR 247	0	−1.60	(-)
TIR 248	0	−2.10	(+)
TIR 249	0	−3.00	(-)
TIR 250	0	−4.00	(+)
TIR 251	0	−5.00	(-)
TIR 252/CIR 304	−0.63	0	(+)
TIR 253/CIR 303	−1.88	0	(+)
TIR 254/CIR 302	−3.13	0	(+)
TIR 255/CIR 301	−4.38	0	(+)
TIR 256/CIR 305	0	0.63	(+)
TIR 257/CIR 306	0	1.88	(+)
TIR 258/CIR 307	0	3.13	(+)
TIR 259/CIR 308	0	4.38	(+)
TIR 260/CIR 309	0.63	0	(+)
TIR 261/CIR 310	1.88	0	(+)
TIR 262/CIR 311	3.13	0	(+)
TIR 263/CIR 312	4.38	0	(+)
TIR 264/CIR 313	0	−0.63	(+)
TIR 265/CIR 314	0	−1.88	(+)
TIR 266/CIR 315	0	−3.13	(+)
TIR 267/CIR 316	0	−4.38	(+)
Pressure sensor			
PIR 103	0	−3.00	(+)
PIR 104	−7.00	−7.00	(+)
PIR 105	−3.00	0	(-)
PIR 106	−2.00	0	(-)
Bolometer			
1	0	−70.0	(+)
2	0	−90.0	(+)
3	0	−110.0	(+)

Table 2
RPT trials performed showing the number of overall and reliable releases, the type of release (release oriented vertically downward 50 cm above the water surface (AV), 30 cm under the water surface (UV), and horizontally 30 cm under the water surface (UH)), and the estimated mass outflow rate range (Habib et al., 2022).

Trial	N° of releases	N° of reliable* releases	Type of release	Mass outflow rate [kg/s]
001	1	0	AV	-
002	8	5	AV	0.30–1.00
003	1	0	AV	-
004	3	2	UV	0.35–0.85
005	2	0	AV	-
006	4	3	UV	0.50–1.20
007	5	3	UV	0.35–0.65
008	3	2	UV	0.55–0.62
009	3	2	UV	0.35–0.70
010	3	2	UV	0.35–0.45
011	3	2	AV	0.45–0.51
012	3	3	AV	0.32–0.58
013	3	3	AV	0.25–0.40
014	2	2	UV	0.31–0.50
015	3	3	UV	0.50–0.75
016	1	1	UV	0.80
017	5	1	AV	0.40
019	2	1	AV	0.80
020	3	1	AV	1.10
021	4	2	UV	0.25–0.76
022	3	2	UV	0.27–0.37
023	3	2	UH	0.53–0.78
024	3	2	UH	0.36–0.55
025	4	2	UH	0.38–0.52

* Release duration > 10 s and released mass > 5 kg.

leveraging the Savitzky-Golay filter's ability to extract meaningful information from noisy sensor measurements, more reliable and precise data can be captured form the outputs of the experimental tests.

3. Results and discussion

3.1. Results of single experimental tests

To provide a comprehensive overview of the results obtained by the instrumentation placed around the basin, the outputs of Trials 013 and 014 are presented in this paragraph. These trials were selected due to their ability to showcase experimental outputs in the event of above water and underwater releases, as well as whether or not hydrogen

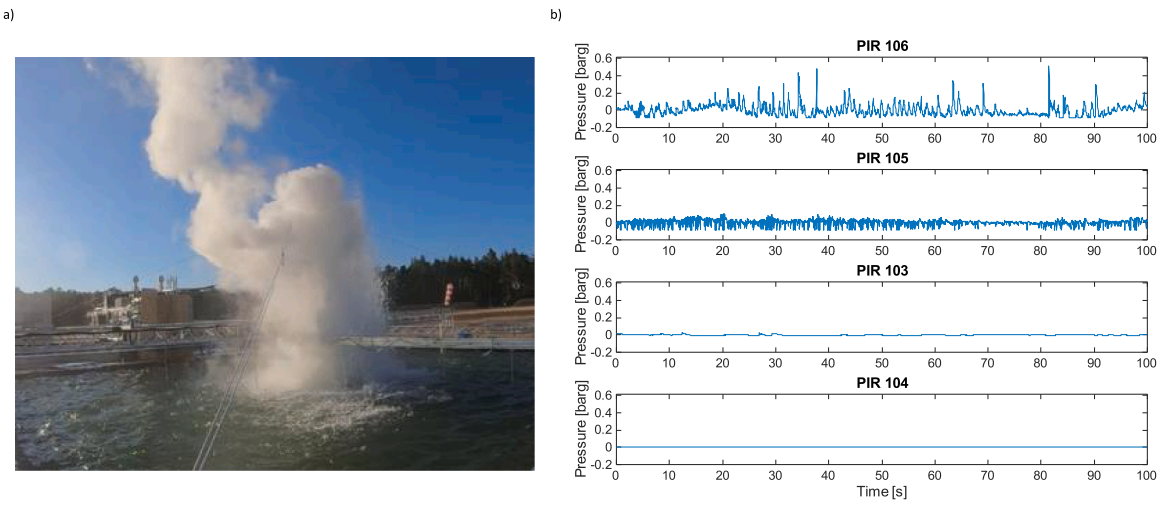

Fig. 3. (a) Evaporation process following the first release of Trial 013 and (b) overpressure results throughout Trial 013 (PIR 103, 3 m away from the release point (in air); PIR 104, 10 m away from the release point (in air); PIR 105, 3 m away from the release point (underwater); PIR 106, 2 m away from the release point (underwater)).

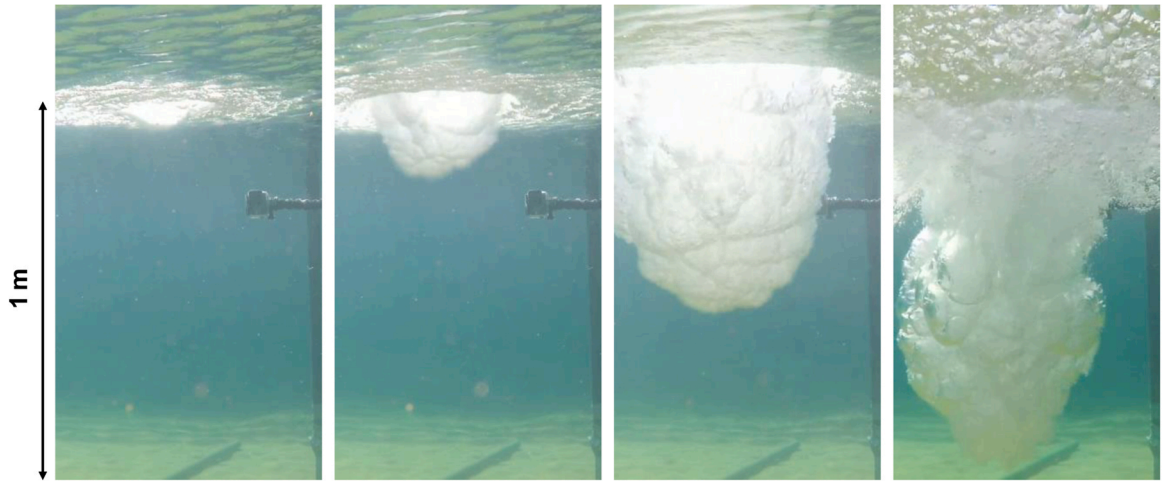

Fig. 4. Multiphase jet progressively penetrating the water and flashing (release of type AV).

gaseous clouds self-ignited after the spillage events.

3.2. Trial 013

Trial 013 comprised three releases of LH_2 above water, oriented vertically downward (type AV), with mass outflow rates ranging from 0.25 kg/s to 0.40 kg/s, and no ignition occurred.

Once the turbulent jet was released from the flexible hose, an immediate evaporation process occurred upon contact with the water. The evaporation was not homogeneous, and frequent geyser-like jets propelled out of the water after the impact, as depicted in Fig. 3(a). Fig. 3(b) reports pressure sensor readings from Trial 013. It is clear that very low overpressures were recorded by PIR 103 and PIR 104, the two aerial pressure sensors. For PIR 106, the underwater blast probe closest to the release point, some higher signals were recorded. However, since PIR 105, the second underwater blast probe in a further distance from the release location, did not show any comparable peaks, it can be concluded that the values recorded from PIR 106 were not caused by pressure waves underwater. Instead, they were due to the resulting "mechanical impacts" on the sensor from the high-momentum gas jet and/or cavitating gas bubbles.

From these readings, it can also be excluded that significant overpressures would result from the simple release of LH_2 onto water when no ignition occurs.

More in detail, as depicted in Fig. 4 (where only a depth up to 1 m was covered by the view angle of the camera in the foreground, although the basin had a total depth of 1.5 m), after the water impact, camera recordings revealed a very chaotic mixing zone that seems to pulsate due to the interplay between volume production from evaporation, insulating bubbles, buoyancy, and the continuously incoming jet. The larger bubbles only formed on the sides of the impact zone, and the vapor layers between LH_2 and water and the bubbles themselves were disintegrated due to what appear to be Taylor instabilities.

The non-stationary evaporation process also affected the gas concentrations in the cloud, resulting in very irregular trends. In fact, as depicted in Fig. 5, the reliable concentration sensors–specifically, CIR 303, CIR 311, and CIR 315 (refer to Fig. 2)–detected hydrogen concentrations in the air up to almost 12 vol%.

Trial 013 is the only one for which self-ignition was not detected for any of the releases, so that no heat radiation signals could be recorded. However, temperatures were detected. For the sake of completeness, Fig. 6 shows all measured temperature data subdivided by the four quadrants of the basin.

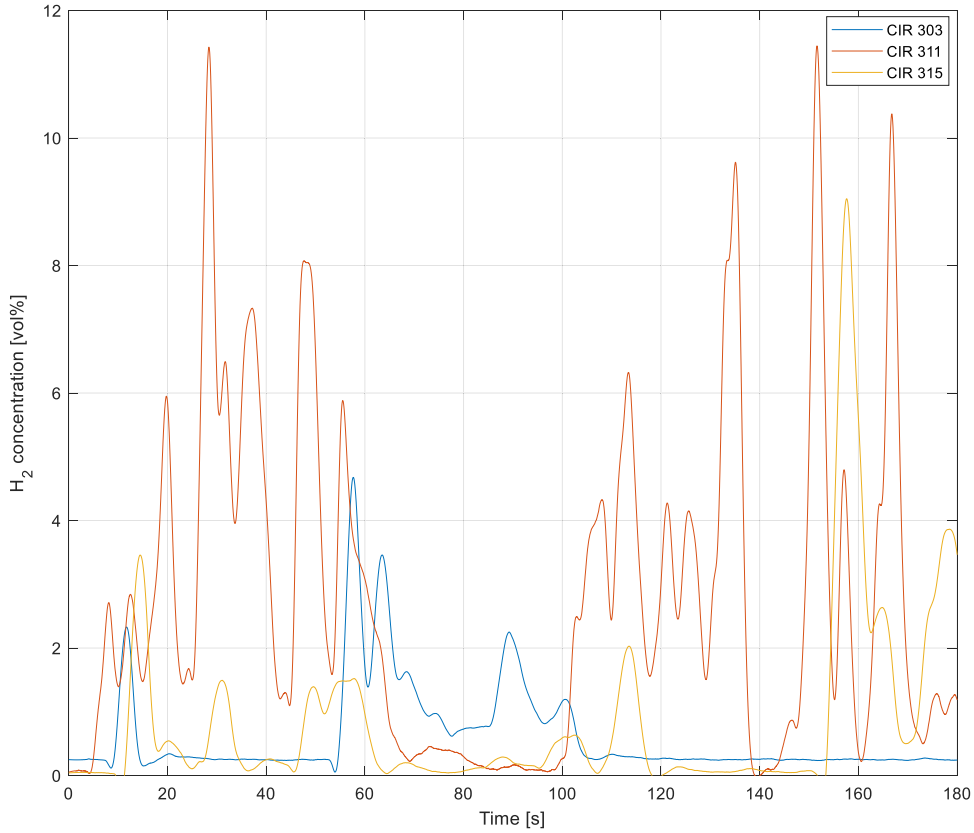

Fig. 5. Trial 013: H_2 concentration results recorded by the reliable sensors CIR 303, CIR 311, and CIR 315.

3.3. Trial 014

Trial 014 consisted of two releases of LH_2 performed underwater and oriented vertically downward (type UV), with mass outflow rates and durations of 0.31 kg/s for 42 s, the first release, and 0.50 kg/s for 71 s, the second release. As mentioned previously regarding Trial 013, once LH_2 is released into the water basin, a considerable degree of flashing occurs, leading to a multiphase jet penetrating deep into the basin. This non-homogeneous evaporation process facilitates the occurrence of several frequent and random jets escaping from the free water surface, as reported in Fig. 7(a).

After respectively 40 s and 69 s from the start of the first and second releases, ignition of the released gaseous clouds was observed. Two seconds elapsed between ignitions and the end of the releases. Fig. 7(b) illustrates the ignited hydrogen-air cloud generated after the second release of Trial 014. Fire durations of approximately 13 s and 10 s were detected for the first and second releases, respectively. Essentially, with increasing outflow rate, the time elapsed before ignition decreases while the fire duration increases.

To better detail the timing of the experimental trial, the following sequence of events (reported in the following figures of this section) can be identified:

I. 0 s: start of the first release;
II. 40 s: ignition of the first release;
III. 42 s: stop of the first release;
IV. 53 s: stop of fire following the first release;
V. 79 s: start of the second release;
VI. 148 s: ignition of the second release;
VII. 150 s: stop of the second release;
VIII. 158 s: stop of fire following the second release.

Similar to the fire duration, temperatures increase with higher outflow rates. Indeed, considering TIR 262 (located in Q3) and TIR 265 (located in Q3), which identified the highest temperature values for the first and second releases, respectively, at increasing outflow rates, the difference between the temperature peaks rises by around 50 °C (refer to Fig. 8). While TIR 262 and TIR 265 identified the highest temperature values, TIR 221 (located in Q2) and TIR 231 (located in Q3) detected the lowest ones (see Fig. 8). It is worth noting that higher values were detected in the water basin quadrant Q3 where the fire spreads after the release, as illustrated in Fig. 7(b).

Although the used thermal cameras were mainly dedicated to provide a representation of the invisible hydrogen flame, a temperature distribution of the flame can also be deduced from the recordings (refer to Fig. 9). It is important to note that these temperature ranges are only a rough estimate, as thermal imaging of flames for the purpose of "measuring" temperature is not possible due to the non-uniform emissivity of the flame and the changing composition of the burning gases, for which no suitable calibration of the (single) camera is possible.

Heat radiation results are reported in Fig. 10. For the first release, values up to approximately 35 W/m^2 were recorded by Bolometer 1, which is the closest to the release point (at 70 m), while for the second release, absolute values of approximately 42 W/m^2 from the baseline were detected by the same instrument.

As expected, the detected heat radiation values decrease with increasing distance of the bolometer from the release point. From the enlargement of Fig. 10, it is possible to see that Bolometer 2 and Bolometer 3, respectively located at 90 m and at 110 m far from the release point, recorded decreasing absolute values of around 15 W/m^2 and 10 W/m^2 from the baseline for the second release of Trial 013.

It is worth noting that heat radiation measurements provided by the bolometers for the first release started from 0 W/m^2 (baseline). In contrast, heat radiation measurements for the second release were influenced by the first release, causing the baseline to shift from 0 W/m^2 to around 7/8 W/m^2. Therefore, it was necessary to scale the heat

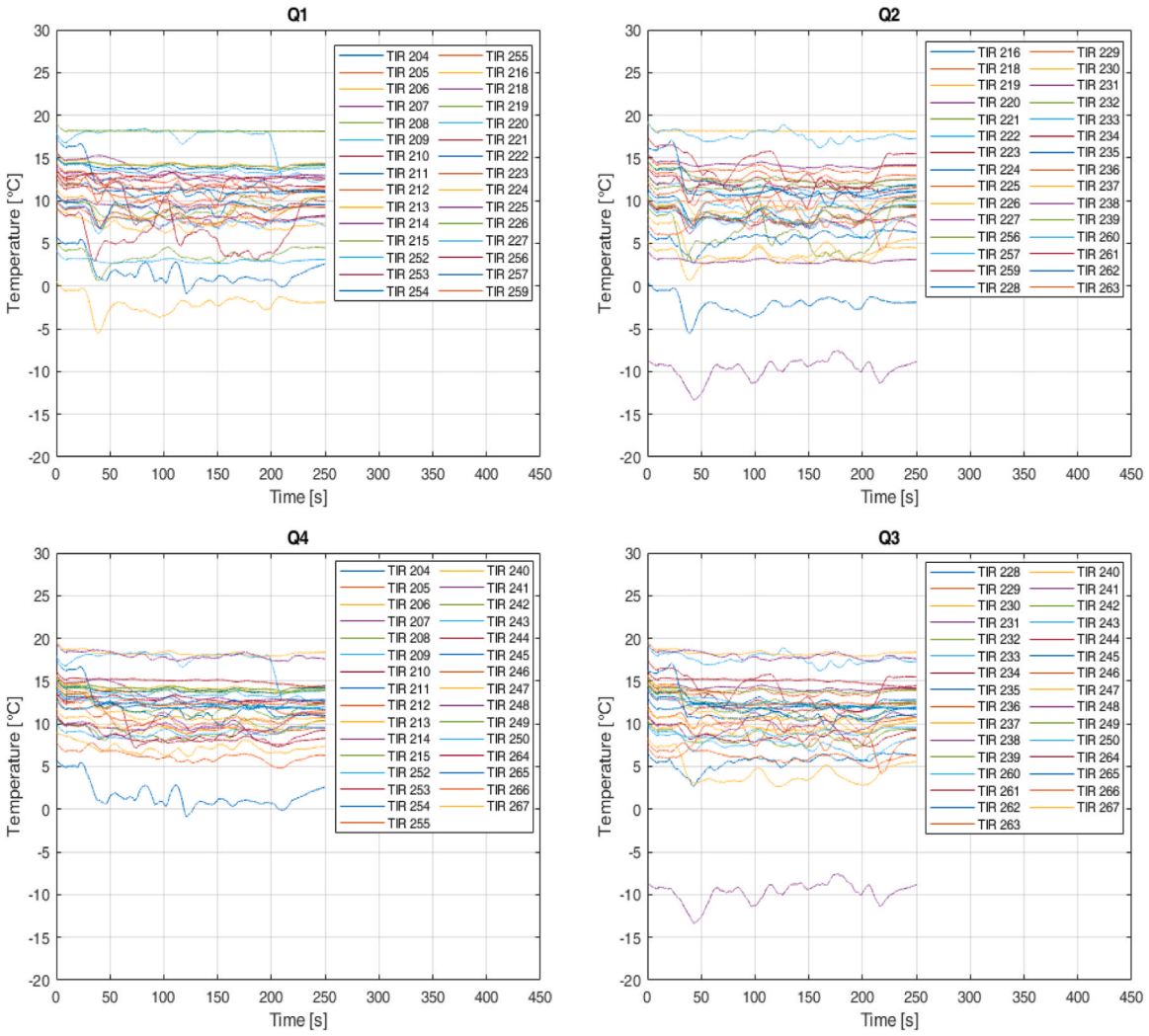

Fig. 6. Trial 013: temperature results subdivided by the four quadrants of the basin.

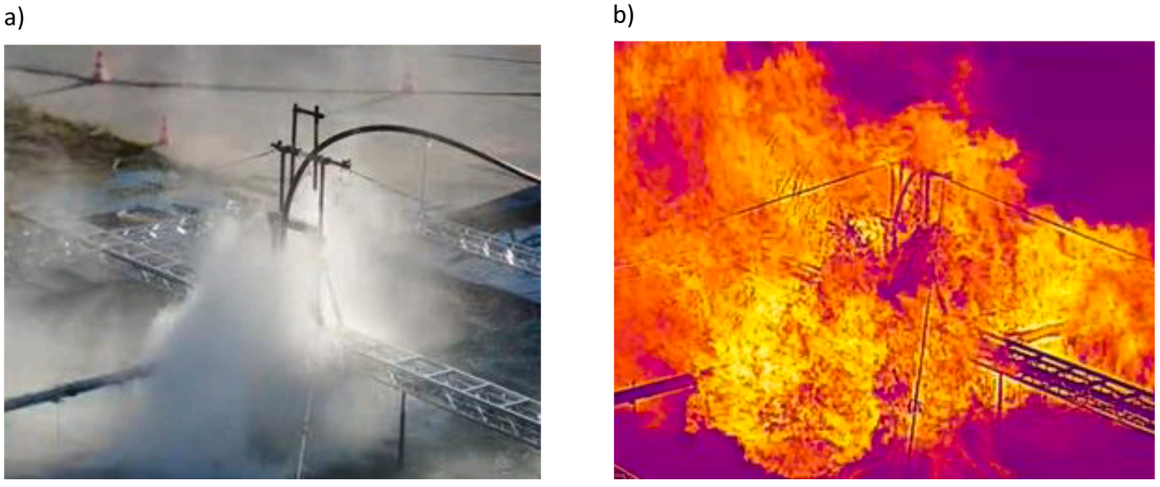

Fig. 7. View of the second LH_2 release of Trial 014: (a) the heterogeneous evaporation of the release at the basin; (b) the thermal camera frame capturing the ignited released gas cloud with fire spreading in quadrant Q3.

radiation values identified for the second release to the baseline (0 W/m^2) to obtain the correct heat radiation values for comparison purposes. The background radiation was measured by a fourth bolometer and subtracted from the heat radiation signals during the data processing, so that the illustrated diagrams are showing the absolute radiation values of the fire.

Strong blast waves in the near field of the release location were detected, as depicted in Fig. 11.

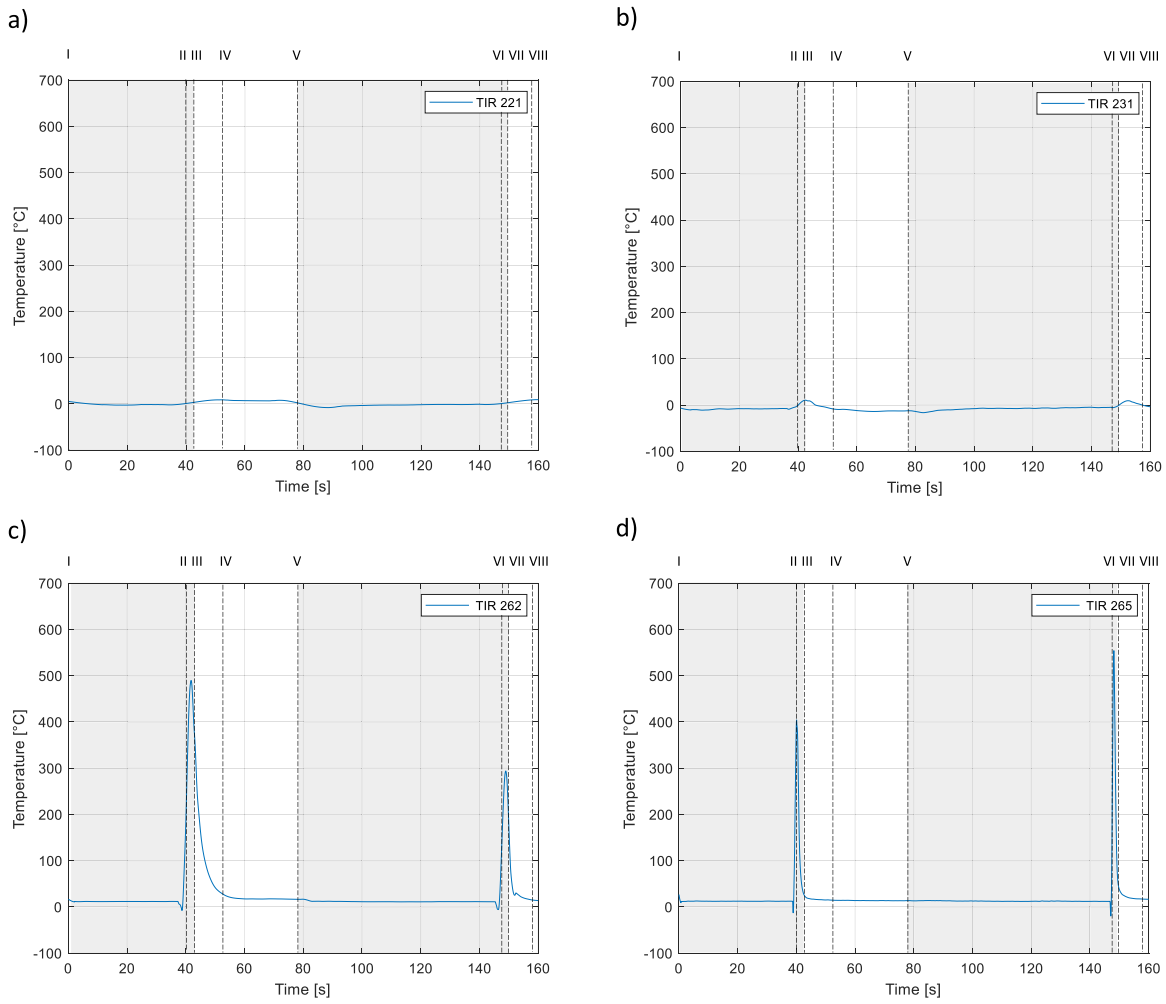

Fig. 8. Trial 014: minimum temperature results recorded by (a) TIR 221 and (b) TIR 231, and maximum temperature results recorded by (c) TIR 262 (first release) and (d) TIR 265 (second release). Gray shadows represent the release durations (1° release from I to III and 2° release from V to VII).

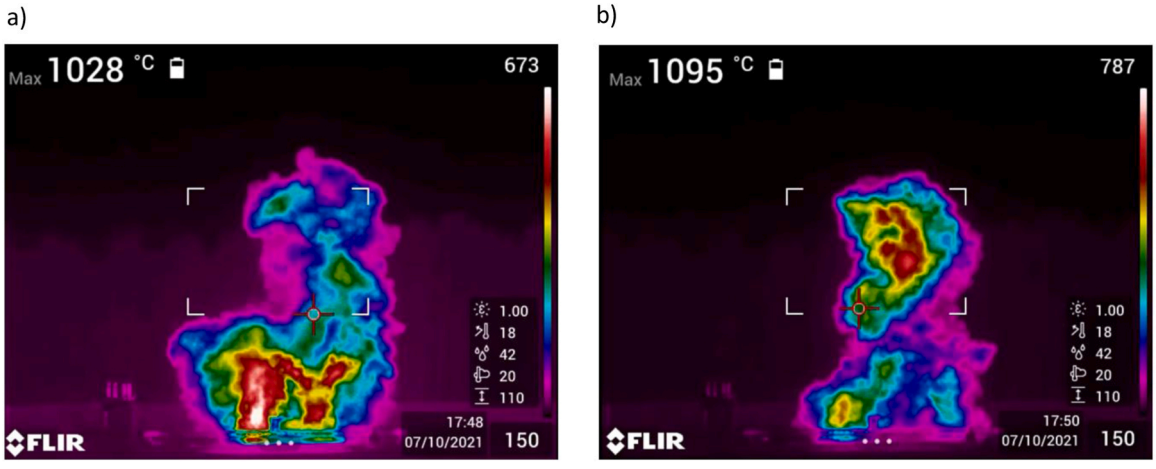

Fig. 9. Trial 014: thermal camera frames of the (a) first and (b) second release with indications of the weather conditions, emissivity assumption, and distance between the flame and the camera.

Blast pressures of up to 1.0 barg and 1.8 barg were measured underwater by PIR 106, the pressure device closest to the release point, specifically 2 m away from it, for the first and second releases, respectively (see Fig. 11(b)). Lower blast pressure values were detected in the air. Specifically, PIR 103 measured overpressure values reaching almost 0.07 barg for the first release and 0.13 barg for the second release (see the enlargement in Fig. 11(a)). In this regard, in Fig. 11(a), two peaks are visible for each release of the trial. However, only the first small peak correctly represents the pressure signal; the following high decrease and increase are only faulty values due to temperature effects of the burning

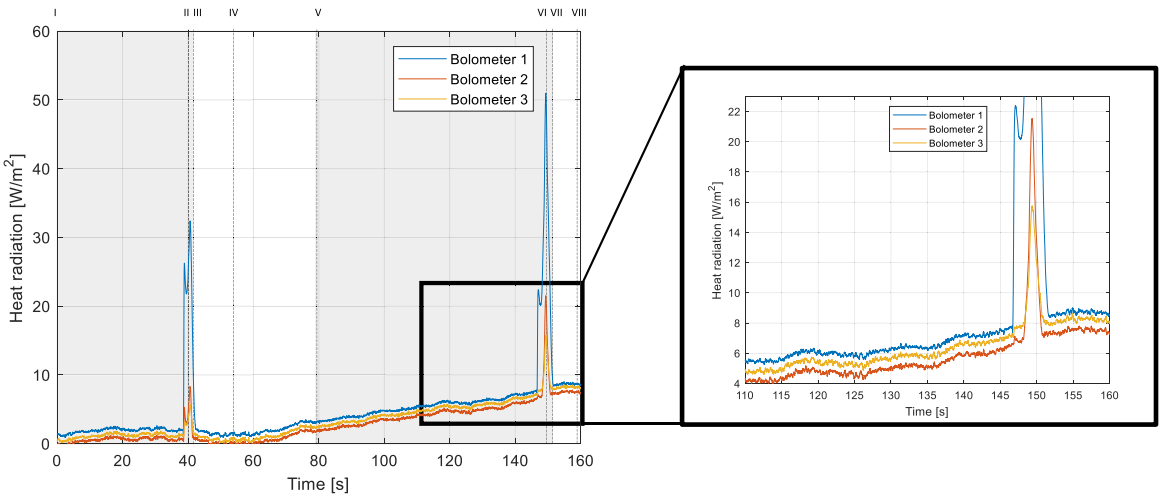

Fig. 10. Trial 014: heat radiation results recorded by bolometer 1, 2, and 3 located at 70 m, 90 m, and 110 m far from the release location, for the first and second releases. Gray shadows represent the release durations (1° release from I to III and 2° release from V to VII).

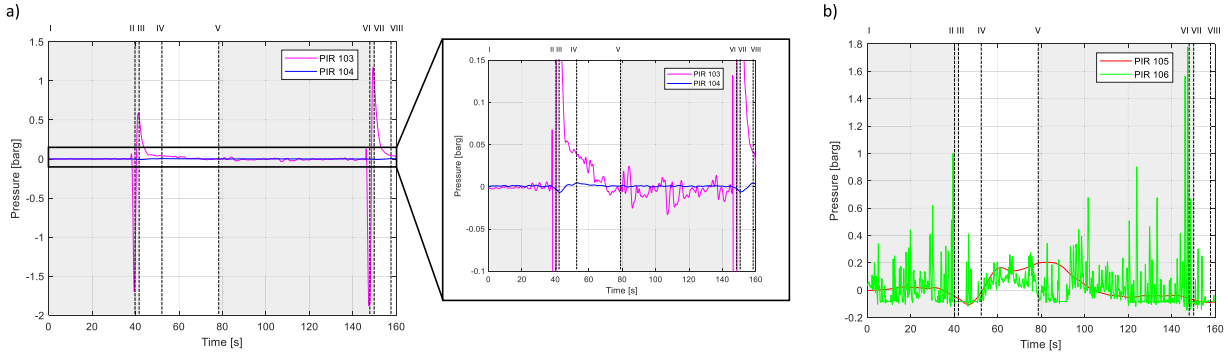

Fig. 11. Trial 014: (a) above water and (b) below water overpressure results (PIR 103, 3 m away from the release point; PIR 104, 10 m away from the release point; PIR 105, 3 m away from the release point; PIR 106, 2 m away from the release point). Gray shadows represent the release durations (1° release from I to III and 2° release from V to VII).

gas cloud on the sensor.

In comparison to the findings from Trial 013 (see Fig. 3(b)), in the case of releases with ignition, pressure events are recorded both underwater and in the air. No direct correlation can be established between the very high underwater (see Fig. 11(b)) and the significantly lower aerial (see Fig. 11(a)) pressure values, especially since all sensors are located in different positions from the release and ignition points. It can only be concluded that ignitions of the gas cloud are accompanied by sensible overpressures in air, as well as higher overpressures underwater, certainly mainly resulting from the underwater evaporation and expansion of the LH_2 jet.

Lastly, the concentration of hydrogen in the air was measured by specific gas sensors placed in correspondence of specific thermocouples. For Trial 014, the H_2 concentration sensors CIR 311 and CIR 314 located respectively near TIR 262 and TIR 265 (i.e., the TIRs measuring the highest temperature values for this trial) recorded concentrations up to 20–25 vol% (refer to (Habib et al., 2022)).

3.4. Ignition of hydrogen-air clouds

The results of the experimental campaign demonstrated that, instead of a pressure effect caused by a pure RPT, self-ignition was observed, followed by a gas cloud explosion and subsequent pressure development. Out of a total of 75 LH_2 releases, 60 resulted in ignition, indicating that 80 % of the releases ignited. A lower percentage can be identified for the reliable ones. Specifically, out of a total of 46 reliable releases, 32 resulted in ignition, representing approximately 70 % of the reliable releases that ignited during the experimental campaign.

Analysing both the ignited overall and reliable releases per type of release, Table 3 illustrates that the majority of ignited releases, regardless of their reliability, are associated with underwater spill events with a vertical downward orientation (UV), followed by underwater releases oriented horizontally parallel to the water surface (UH) and above water releases oriented vertically downward (AV).

After a general overview regarding the ignition phenomenon affecting the trials, specific data related to the individual ignited reliable

Table 3
Percentages of ignited overall and reliable releases per type of release.

Type of release	N° of overall releases	N° of overall ignitions	Percentage of ignited overall releases	N° of reliable releases	N° of reliable ignitions	Percentage of ignited reliable releases
AV	31	21	68 %	16	6	38 %
UV	34	32	94 %	24	23	96 %
UH	10	7	70 %	6	3	50 %

Table 4
Collection of ignition data related to the individual reliable releases: experimental sequence number of the ignited release, outflow rate of the ignited release, time elapsed before ignition after the start of the release, fire duration, and maximum heat radiation value measured during the release.

Trial	Sequence number of the ignited release	Ignited mass outflow rate [kg/s]	Ignition time [s]	Fire duration [s]	Maximum heat radiation value* [W/m^2]
002	7	0.77	36	26	n.a.
002	8	0.59	19	27	n.a.
004	2	0.84	10	7	n.a.
004	3	0.34	25	7	n.a.
006	1	1.09	9	38	60
006	3	1.19	9	11	80
006	4	0.51	22	8	67
007	1	0.65	18	10	80
007	4	0.35	8	8	64
007	5	0.45	41	8	59
008	1	0.56	43	26	48
008	3	0.61	20	7	62
009	1	0.35	14	7	51
009	3	0.70	36	8	64
010	1	0.45	10	7	64
012	1	0.58	7	33	79
014	1	0.31	40	13	32
014	2	0.50	69	10	42
015	1	0.51	10	34	73
015	2	0.60	10	47	115
015	3	0.75	27	12	87
016	1	0.79	8	15	110
017	5	0.42	11	36	104
019	2	0.82	11	65	95
020	2	1.10	19	64	132
021	1	0.76	36	7	80
021	2	0.26	21	6	105
022	1	0.37	14	6	125
022	2	0.27	28	7	73
023	2	0.78	11	23	82
024	1	0.36	37	6	85
025	4	0.38	35	6	45

* Value measured from the baseline (0 W/m^2) by Bolometer 1 located at 70 m from the release point; n.a. = not available (due to bolometers switched off).

releases were reported in Table 4.

Basically, as the outflow rate increases, momentum increases, and ignition probability rises. Indeed, the velocity of the release at the outlet section of the flexible hose increases with the outflow rate, consequently enhancing the subsequent evaporation process. Camera recordings revealed increasingly massive evaporation with rising outflow rates.

Based on this and by plotting the ignition data collected in Table 4, the trends suggest that as the mass outflow rate increases, the ignition time tends to decrease while the fire duration increases (refer to Fig. 12 (a) and Fig. 12(b)). However, these relationships are not fully reflected in the plotted data due to the scattered behaviour, which is linked to inaccuracies in the truck weighing process during the trials, caused by wind conditions and the specific wind load on the truck trailer. More precise tests will likely confirm the trends.

Furthermore, for higher released masses and outflow rates, the flame dimensions of the ignited cloud increase, as depicted in Fig. 13. In fact, moving from Fig. 13(a) to Fig. 13(b), where the released mass (or mass outflow rate) increases from 5.44 kg (or 0.51 kg/s) to 22.8 kg (or 0.75 kg/s) under comparable atmospheric conditions (i.e., no changes in wind specifications), the thermal camera frames illustrate a corresponding increase in the maximum extension of the flames.

To exclude that potential ignition sources could originate from the instrumentation placed around the basin despite previous grounding operations, Trials 015, 016, and 017 were conducted with all measuring technology switched off, except for cameras and bolometers. However, these devices were placed far from the release point, thus unable to contribute as potential ignition sources. Nevertheless, ignition was still observed during these trials, proving that the ignition source did not originate from the measuring equipment. Detailed examination of the IR video recordings showed that the ignition source was located "*in free air*" within the gas cloud. In Fig. 14, the location of the ignition source is represented by the "white spot". A potential explanation of this phenomenon could be corona discharges at ice crystals developing from the release/evaporation process due to the very low minimum ignition energy of hydrogen. However, further investigation of this experimental finding is necessary to evaluate the reliability of this theory.

Trials 001, 002, 003, 004, and 022 were executed without bolometers being switched on; therefore, no results in terms of heat radiation were provided. However, for all the other trials, heat radiation values of up to 132 W/m^2 were detected at the bolometer locations for the trials with ignition (see the sixth column of Table 4). Radiation levels of concern close to 150 W/m^2 (Atallah and Allan, 1971) likely only appear very close to the flames. Overall, higher heat radiation values were identified for releases of type AV compared to the underwater ones. This is quite obvious since in above water releases, the flame remains largely above the water, producing more intense radiation. Conversely, in underwater releases, gas loses momentum as it is entrained in the water before rising to the surface, naturally resulting in lower heat radiation.

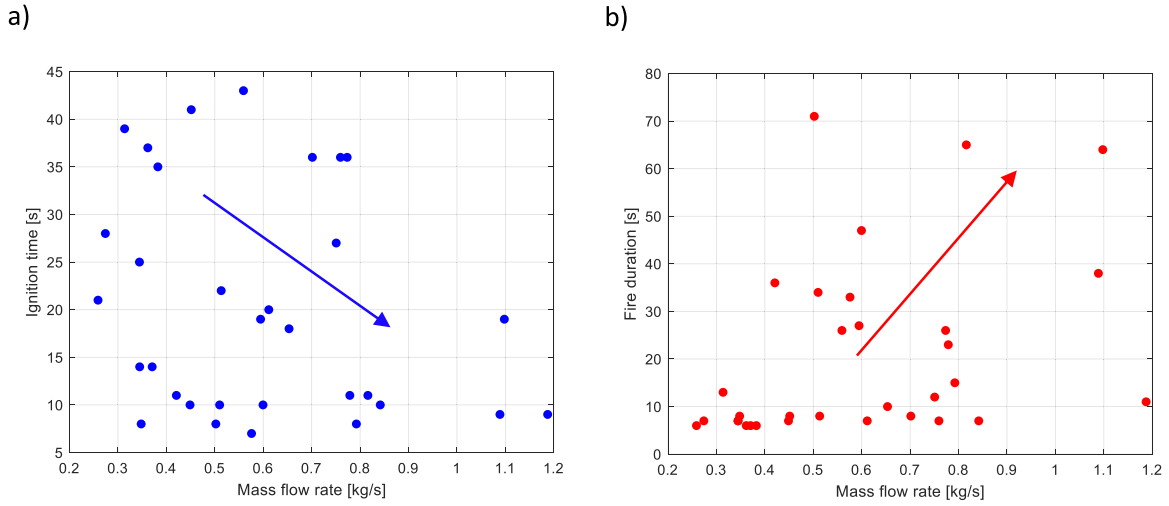

Fig. 12. a) Ignition time and b) fire duration as a function of the mass outflow rate for the ignited reliable releases.

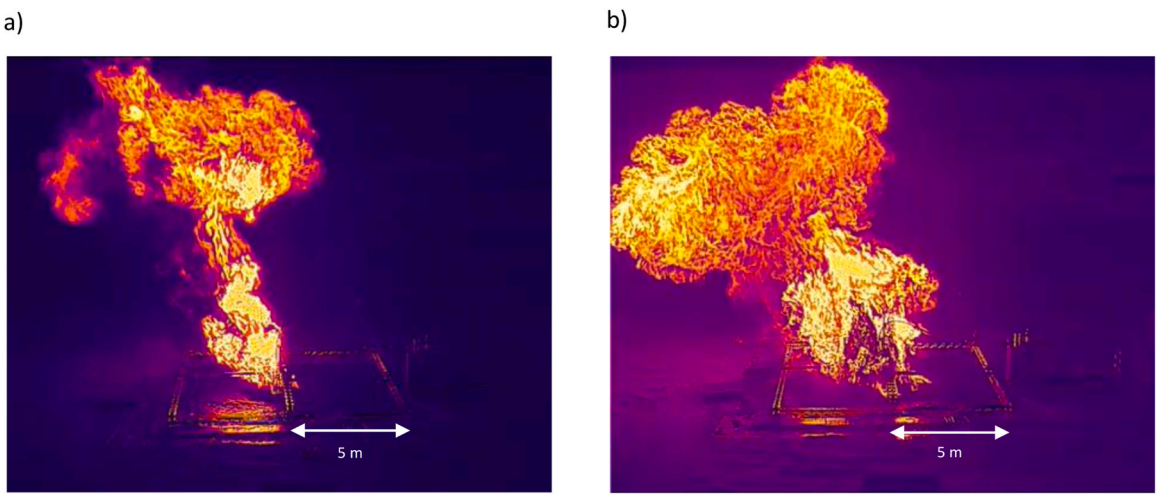

Fig. 13. Thermal camera frames capturing the steady state flames identified during Trial 015: (a) first release with a released mass of 5.44 kg and an outflow rate of 0.51 kg/s, and (b) third release with a released mass of 22.80 kg and an outflow rate of 0.75 kg/s.

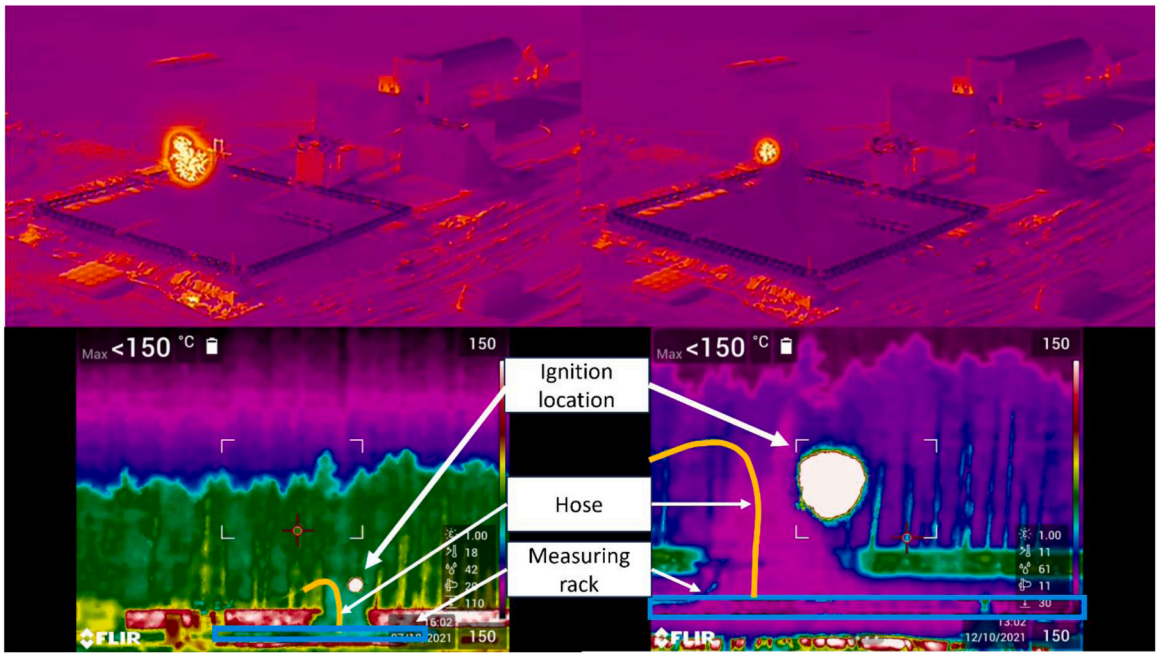

Fig. 14. Start of flame propagation in hydrogen-air clouds ("white spots") generated by releases of LH_2 (Habib et al., 2022).

3.5. *Overpressure generated in experimental trials*

The blast pressure generated after the releases was measured both underwater and in the air. For Trials 001, 002, 003, and 004 no pressure values are available, same as for Trials 015, 016, and 017, where, as mentioned before, the measuring equipment was switched off. However, results were available for all the other experimental tests. Due to the ignition phenomenon, very erratic trends were observed in the pressure probes (see, for instance, Fig. 15). Subsonic flame propagation velocities in the order of 100–200 m/s were encountered, indicating a very turbulent cloud that generates an explosion classified as deflagration (TNO, 2005). Moreover, several overpressure peaks were detected during the same release. The duration of some of these peaks appeared long compared to typical explosions lasting milliseconds, influencing the magnitude of the impulse as shown in the enlargement in Fig. 15.

In the following, in Fig. 16, overpressure data were reported as a function of the outflow rate for all the ignited reliable releases of the different experimental tests. Specifically, in Fig. 16(a), the overpressure results detected in air by PIR 103 and PIR 104 are reported, while in Fig. 16(b), the overpressure results detected underwater by PIR 105 and PIR 106 are collected.

From the graphs it is possible to state that no correlations between the mass flow rate and the overpressure values exist. Comparing the above and underwater overpressure data, the underwater ones were much higher than the ones detected in the air. Values of up to 0.35 barg were recorded by PIR 103 (see Fig. 16(a)), the closest aerial pressure probe to the release point (3 m), and up to 3.5 barg by PIR 106 (see Fig. 16(b)), the closest underwater sensor (2 m). However, these two values seem to be exceptional cases. In fact, lower values up to 0.15 barg and 1 barg were generally recorded by PIR 103 (see Fig. 16(a)) and PIR 106 (see Fig. 16(b)), respectively. As mentioned in Section 3.1.2, ignition of the gas cloud impacts the aerial measurements, but not the underwater ones. The higher values recorded by the underwater pressure sensors are attributed to the overpressures generated by the evaporation

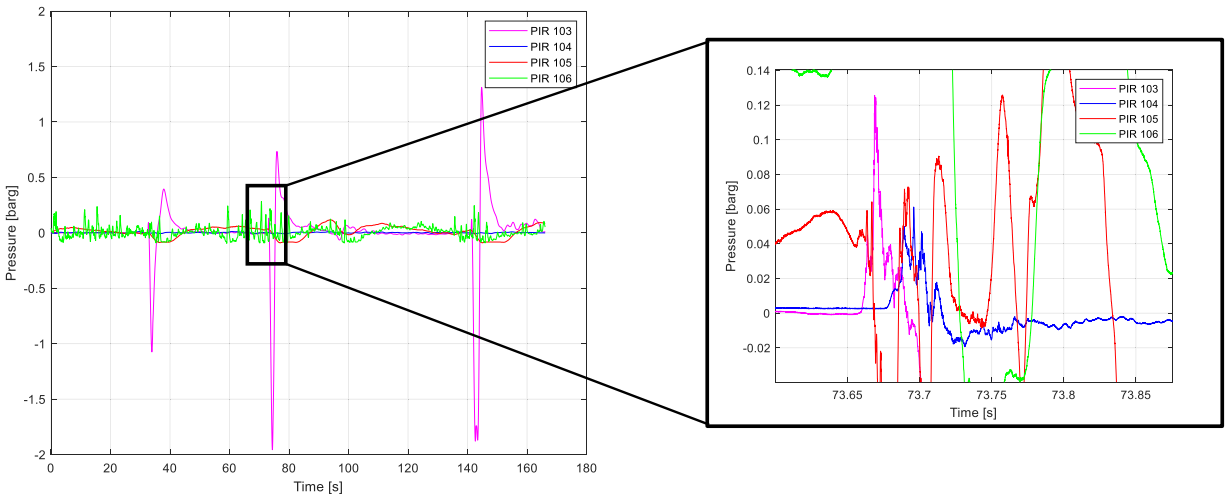

Fig. 15. Trial 021: overpressure results (PIR 103, 3 m away from the release point (in air); PIR 104, 10 m away from the release point (in air); PIR 105, 3 m away from the release point (underwater); PIR 106, 2 m away from the release point (underwater)).

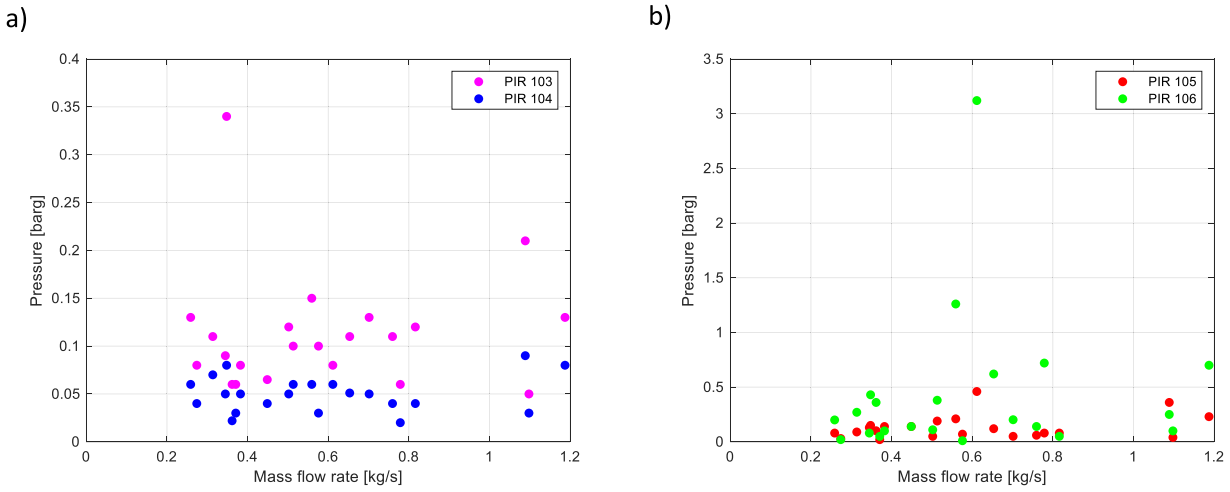

Fig. 16. (a) Above water and (b) underwater overpressure results as a function of the mass outflow rate for the ignited reliable releases (PIR 103, 3 m away from the release point; PIR 104, 10 m away from the release point; PIR 105, 3 m away from the release point; PIR 106, 2 m away from the release point).

and expansion of the LH_2 jet.

For the unignited releases, no overpressures could be detected. While the possibility of RPT occurring and generating overpressures cannot be completely ruled out, any such overpressures would have been so minor that they blended into the background noise of the signal. As a result, even if RPT events did take place, the overpressures they produced were too weak to be distinguished from the surrounding noise, making it impossible to definitively identify or confirm any such event.

4. Conclusions

In the current paper, the experimental tests conducted under the SH_2IFT project, aimed at investigating the behaviour of LH_2 once it is released above or below the water surface, were presented and discussed. From these experiments, on one hand, it was possible to assert that rapid phase transitions (RPTs) resulting from LH_2 spills onto or into water are not a significant concern for the safe implementation of LH_2 technologies. The theoretical pathways known for the LNG research are very unlikely or even impossible for LH_2, primarily due to the very low Leidenfrost temperature of LH_2, which keeps the vapor film between LH_2 and water stable. However, more research on film-boiling stability for high-impact forces and in chaotic mixing regions is needed to understand triggering of early RPTs more fundamentally. On the other hand, ignition events emerged as a primary issue, despite the absence of theoretical ignition sources in the experimental field. Remarkably, spills of LH_2 into water exhibit the highest ignition rate, highlighting the potential danger associated with such scenarios. Consequently, efforts should be directed towards minimizing these occurrences, as the resultant flammable cloud can lead to violent explosions upon ignition. The dataset results highlighted significant increases in pressure in the surrounding area and underwater. While excess pressures of up to 0.35 barg were measured on land, the values measured underwater were close to 3.5 barg.

The insights gleaned from the experimental dataset have significant implications for operational practices and risk mitigation strategies. By integrating the findings into safety protocols, the industry can notably enhance the safety and efficiency of LH_2 management. This proactive approach not only mitigates risks, but also fosters continuous safety improvement in the field of hydrogen technologies.

Overall, the study underscores the importance of conducting rigorous experimentation and analysis to advance safety standards and deepen our understanding of hydrogen technology. By addressing key safety concerns and leveraging empirical data, stakeholders can collectively work towards a safer and more sustainable future for LH_2

utilization, ensuring its integration into various sectors while mitigating associated risks.

CRediT authorship contribution statement

Federico Ustolin: Writing – review & editing, Visualization, Supervision, Methodology. **Abdel Karim Habib:** Writing – review & editing, Visualization, Validation, Resources, Data curation. **Nicola Paltrinieri:** Writing – review & editing, Supervision, Funding acquisition. **Valerio Cozzani:** Writing – review & editing, Supervision. **Martin Kluge:** Writing – review & editing, Visualization, Validation, Resources, Data curation. **Federica Tamburini:** Writing – original draft, Visualization, Methodology, Investigation, Formal analysis, Data curation, Conceptualization.

Declaration of Competing Interest

The authors declare that they have no known competing financial interests or personal relationships that could have appeared to influence the work reported in this paper.

Acknowledgments

This work was undertaken as part of the research project Safe Hydrogen fuel handling and Use for Efficient Implementation 2 (SH_2IFT-2). The authors would like to acknowledge the financial support of the Research Council of Norway (under the ENERGIX programme (Grant No. 327009)), Air Liquide, Equinor, Shell, Safetec, Total and a number of Norwegian municipalities.

References

Abbass, K., Qasim, M.Z., Song, H., Murshed, M., Mahmood, H., Younis, I., 2022. A review of the global climate change impacts, adaptation, and sustainable mitigation measures. Environ. Sci. Pollut. Res. 29, 42539–42559. https://doi.org/10.1007/s11356-022-19718-6.

Abohamzeh, E., Salehi, F., Sheikholeslami, M., Abbassi, R., Khan, F., 2021. Review of hydrogen safety during storage, transmission, and applications processes. J. Loss Prev. Process Ind. 72, 104569. https://doi.org/10.1016/j.jlp.2021.104569.

Ahluwalia, R.K., Peng, J.K., Roh, H.S., Papadias, D., Wang, X., Aceves, S.M., 2023. Liquid hydrogen storage system for heavy duty trucks: capacity, dormancy, refueling, and discharge. Int. J. Hydrog. Energy 48, 34120–34131. https://doi.org/10.1016/j.ijhydene.2023.05.113.

Atallah, S., Allan, D.S., 1971. Safe separation distances from liquid fuel fires. Fire Technol. 7, 47–56. https://doi.org/10.1007/BF02588942.

Atkinson, G., 2020. Experiments and Analyses on Condensed Phases. Report project Prenormative Research for Safe use of Liquid Hydrogen (PRESLEY). Fuel Cells and Hydrogen Joint Undertaking.

Aursand, E., Hammer, M., 2018. Predicting triggering and consequence of delayed LNG RPT. J. Loss Prev. Process Ind. 55, 124–133. https://doi.org/10.1016/j.jlp.2018.06.001.

Aziz, M., 2021. Liquid hydrogen: a review on liquefaction, storage, transportation, and safety. Energies 14. https://doi.org/10.3390/en14185917.

Berstad, D., Gardarsdottir, S., Roussanaly, S., Voldsund, M., Ishimoto, Y., Nekså, P., 2022. Liquid hydrogen as prospective energy carrier: a brief review and discussion of underlying assumptions applied in value chain analysis. Renew. Sustain. Energy Rev. 154, 111772. https://doi.org/10.1016/j.rser.2021.111772.

Fawzy, S., Osman, A.I., Doran, J., Rooney, D.W., 2020. Strategies for mitigation of climate change: a review. Environ. Chem. Lett. 18, 2069–2094. https://doi.org/10.1007/s10311-020-01059-w.

Habib, A.K., Kluge, M., van Wingerden, K., 2022. Experimental investigation into the consequences of release of liquified hydrogen onto and under water, in: Beyer, M., Lucassen, A (Eds.), Proc. of the 14th International Symposium on Hazards, Prevention and Mitigation of Industrial Explosions. Bundesanstalt fuer Materialforschung und -pruefung (BAM), Berlin, Germany, 182–196.

Hansen, O.R., 2020. Hydrogen infrastructure—efficient risk assessment and design optimization approach to ensure safe and practical solutions. Process Saf. Environ. Prot. 143, 164–176. https://doi.org/10.1016/j.psep.2020.06.028.

Hassan, Q., Algburi, S., Jaszczur, M., Al-Jiboory, A.K., Al Musawi, T.J., Ali, B.M., Viktor, P., Fodor, M., Ahsan, M., Salman, H.M., Sameen, A.Z., 2024. Hydrogen role in energy transition: a comparative review. Process Saf. Environ. Prot. 184, 1069–1093. https://doi.org/10.1016/j.psep.2024.02.030.

IEA, 2023. World Energy Outlook.

IPCC, 2005. IPCC Spec. Rep. Carbon Dioxide Capture Storage, 10.1016/bs.ache.2021.10.005.

Isnanto, R., 2011. Comparation on several smoothing methods in nonparametric regression. J. Sist. Kompter 1, 41–47.

John, A., Sadasivan, J., Seelamantula, C.S., 2021. Adaptive Savitzky-Golay filtering in Non-Gaussian noise. IEEE Trans. Signal Process. 69, 5021–5036. https://doi.org/10.1109/TSP.2021.3106450.

Li, H., Cao, X., Liu, Y., Shao, Y., Nan, Z., Teng, L., Peng, W., Bian, J., 2022. Safety of hydrogen storage and transportation: an overview on mechanisms, techniques, and challenges. Energy Rep. 8, 6258–6269. https://doi.org/10.1016/j.egyr.2022.04.067.

Mangold, J., Silberhorn, D., Moebs, N., Dzikus, N., Hoelzen, J., Zill, T., Strohmayer, A., 2022. Refueling of LH2 aircraft—assessment of turnaround procedures and aircraft design implication. Energies 15, 2475.

Menon, S.V., Seelamantula, C.S., 2014. Robust Savitzky-Golay filters. Int. Conf. Digit. Signal Process. DSP 688–693. https://doi.org/10.1109/ICDSP.2014.6900752.

Nukusheva, A., Ilyassova, G., Rustembekova, D., Zhamiyeva, R., Arenova, L., 2021. Global warming problem faced by the international community: international legal aspect. Int. Environ. Agreem. Polit. Law Econ. 21, 219–233. https://doi.org/10.1007/s10784-020-09500-9.

Ødegård, A., Sommerseth, C., Odsæter, L.H., Skarsvåg, H.L., Nekså, P., Meraner, C., Stølen, R., Li, T., Muthusamy, D., Van Wingerden, K., Siccama, D., Gawas, Y., Ustolin, F., Cyriac, G., 2022. D5.4: SH2IFT Final Project Report.

Odsæter, L.H., Skarsvåg, H.L., Aursand, E., Ustolin, F., Reigstad, G.A., Paltrinieri, N., 2021. Liquid hydrogen spills on water—risk and consequences of rapid phase transition. Energies 14, 1–15.

Olabi, A.G., Abdelkareem, M.A., Mahmoud, M.S., Elsaid, K., Obaideen, K., Rezk, H., Wilberforce, T., Eisa, T., Chae, K.J., Sayed, E.T., 2023. Green hydrogen: pathways, roadmap, and role in achieving sustainable development goals. Process Saf. Environ. Prot. 177, 664–687. https://doi.org/10.1016/j.psep.2023.06.069.

Pasman, H.J., Rogers, W.J., 2012. Risk assessment by means of Bayesian networks: a comparative study of compressed and liquefied H 2 transportation and tank station risks. Int. J. Hydrog. Energy 37, 17415–17425. https://doi.org/10.1016/j.ijhydene.2012.04.051.

Pleshivtseva, Y., Derevyanov, M., Pimenov, A., Rapoport, A., 2023. Comprehensive review of low carbon hydrogen projects towards the decarbonization pathway. Int. J. Hydrog. Energy 48, 3703–3724. https://doi.org/10.1016/j.ijhydene.2022.10.209.

Reigstad, G.A., Roussanaly, S., Straus, J., Anantharaman, R., de Kler, R., Akhurst, M., Sunny, N., Goldthorpe, W., Avignon, L., Pearce, J., Flamme, S., Guidati, G., Panos, E., Bauer, C., 2022. Moving toward the low-carbon hydrogen economy: experiences and key learnings from national case studies. Adv. Appl. Energy 8, 100108. https://doi.org/10.1016/j.adapen.2022.100108.

Rong, Y., Peng, J., Gao, J., Zhang, X., Li, X., Pan, X., Chen, J., Chen, S., 2023. Numerical investigation on the liquid hydrogen leakage and protection strategy. Processes 11, 1173. https://doi.org/10.3390/pr11041173.

Salzano, E., Carboni, M., Pio, G., 2020. The effects of low-temperature phenomena on rapid phase transition of liquid hydrogen. Int. J. Hydrog. Energy 45, 32676–32685. https://doi.org/10.1016/j.ijhydene.2020.08.140.

Shu, Z., Lei, G., Liang, W., Dai, W., Lu, F., Zheng, X., Qian, H., 2022. Experimental investigation of hydrogen dispersion characteristics with liquid helium spills in moist air. Process Saf. Environ. Prot. 162, 923–931. https://doi.org/10.1016/j.psep.2022.04.066.

Tamburini, F., Bonvicini, S., Cozzani, V., 2023a. Risk of Subsea blowouts in marine CCS. Chem. Eng. Trans. 99, 265–270. https://doi.org/10.3303/CET2399045.

Tamburini, F., Bonvicini, S., Cozzani, V., 2024a. Consequences of subsea CO2 blowouts in shallow water. Process Saf. Environ. Prot. 183, 203–216. https://doi.org/10.1016/j.psep.2024.01.008.

Tamburini, F., Ricci, F., Tzioutzios, D., Paltrinieri, N., 2024b. Understanding Natech accident scenarios at Carbon capture and storage (CCS) Plants. Chem. Eng. Trans. 111, 391–396. https://doi.org/10.3303/CET24111066.

Tamburini, F., Sgarbossa, F., Cozzani, V., Paltrinieri, N., 2023. Task analysis and human error identification to improve the liquid hydrogen bunkering process in the maritime sector, in: Proc. of ESREL2023, 647–654. doi:10.3850/978-981-18-8071-1_p492-cd.

Tamburini, F., Ustolin, F., Cozzani, V., Paltrinieri, N., 2024. Performance assessment of safety barriers in liquid hydrogen bunkering operations using Bayesian network, in: Proc. of the ASME 2024 43rd International Conference on Ocean, Offshore and Arctic Engineering, OMAE2024, 1–9. doi: 10.1115/OMAE2024-126832.

Tamburini, F., Ustolin, F., Salzano, E., Cozzani, V., Paltrinieri, N., 2023. Lessons learned from experimental tests concerning liquid hydrogen releases, in: Institution of Chemical Engineers Symposium Series.

Tamburini, F., Zanobetti, F., Cipolletta, M., Bonvicini, S., Cozzani, V., 2024d. State of the art in the quantitative risk assessment of the CCS value chain. Process Saf. Environ. Prot. 191, 2044–2063. https://doi.org/10.1016/j.psep.2024.09.066.

The MathWorks Inc, 2024. Matlab R2024a.

TNO, 2005. Methods for the calculation of physical effects (yellow book). Publ. Ser. Danger. Subst.

Ustolin, F., Campari, A., Taccani, R., 2022. An extensive review of liquid hydrogen in transportation with focus on the maritime sector. J. Mar. Sci. Eng. 10. https://doi.org/10.3390/jmse10091222.

Ustolin, F., Odsæter, L.H., Reigstad, G., Skarsvåg, H.L., Paltrinieri, N., 2020a. Theories and mechanism of rapid phase transition. Chem. Eng. Trans. 82, 253–258. https://doi.org/10.3303/CET2082043.

Ustolin, F., Paltrinieri, N., Berto, F., 2020b. Loss of integrity of hydrogen technologies: a critical review. Int. J. Hydrog. Energy 45, 23809–23840. https://doi.org/10.1016/j.ijhydene.2020.06.021.

Verfondern, K., Dienhart, B., 2007. Pool spreading and vaporization of liquid hydrogen. Int. J. Hydrog. Energy 32, 2106–2117. https://doi.org/10.1016/j.ijhydene.2007.04.015.

Wang, F., Li, X., Wu, S., Zheng, L., Luo, Q., Zhang, J., Barbieri, D.M., 2023. Comparative study for global warming potentials of Chinese and Norwegian roads with life cycle assessment. Process Saf. Environ. Prot. 177, 1168–1180. https://doi.org/10.1016/j.psep.2023.07.063.

Zhang, T., Uratani, J., Huang, Y., Xu, L., Griffiths, S., Ding, Y., 2023. Hydrogen liquefaction and storage: recent progress and perspectives. Renew. Sustain. Energy Rev. 176, 113204. https://doi.org/10.1016/j.rser.2023.113204.